Icarus 207 (2010) 686–698

Contents lists available at ScienceDirect

Icarus

journal homepage: www.elsevier.com/locate/icarus

Characterization of fluvial activity in Parana Valles using different age-dating techniques

S. Bouley [a,b,c,*], R.A. Craddock [a], N. Mangold [c], V. Ansan [c]

[a] Center for Earth and Planetary Studies, National Air and Space Museum, Smithsonian Institution, Washington, DC 20560-0315, United States
[b] IDES, UMR8148, Bat. 509, Université Paris XI, 91405 Orsay Cedex, France
[c] LPG Nantes, UMR6112 CNRS, 44322 Université Nantes, France

ARTICLE INFO

Article history:
Received 21 July 2009
Revised 13 November 2009
Accepted 22 December 2009
Available online 18 January 2010

Keyword:
Mars

ABSTRACT

Martian valley networks provide the best evidence that the climate on Mars was different in the past. Although these features are located primarily in heavily cratered terrain of Noachian age (>3.7 Ga), the ages of the features and the time when they were active is not well understood. From superposed craters several recent global studies determined that most valley networks formed during the Late Noachian to Early Hesperian; however, there were some disparities between the techniques. In this study, our principal objective was to test the reliability of the different age-dating techniques to better understand their accuracy and limitations. We applied these techniques to Parana Valles using a variety of high-resolution images taken from different instruments that allow us to identify smaller craters ($D > 125$ m) while providing sufficient coverage to support a statistically reliable sampling of crater populations, which is necessary to reduce the uncertainties in age determination. Our results indicate that Parana Valles formed during the Early Hesperian Period but that the crater density ($D > 353$ m) is heterogeneous inside the Parana Valles basin. The crater population decreases from the headwaters downstream recording a resurfacing event that is most likely related to the erosion of downstream sub-basins. The terrain near the source area is Late Noachian to Early Hesperian in age while terrains closer to the outlet are Early to Late Hesperian in age. Crater densities ($D > 125$ m) inside the valley are also heterogeneous and record several resurfacing events on the valley floor. Where the width of the valley network narrows to <2 km we found evidence of an Amazonian age eolian deposit that is a relatively thin layer of only few meters that was probably deposited as a result of topographic influences. Our results validate the reliability of several proposed age-dating techniques, but we also determined the accuracy and applicability of these techniques. Our results also demonstrate that crater populations can be used to not only determine the relative ages of valley networks, but also to map the distribution of sedimentary materials and the extent of resurfacing events that occurred after valley network formation.

1. Introduction

Martian valley networks, which are located primarily in the heavily cratered terrain on Mars (e.g. Milton, 1973; Schultz and Ingerson, 1973; Sharp and Malin, 1975; Carr and Clow, 1981; Mars Channel Working Group, 1983; Carr, 1996) are the best evidence that liquid water may have been stable on the surface at one time and that the past climate may have been warmer than today (Carr, 1981; Gulick, 2001; Craddock and Howard, 2002). Because they are located primarily in Noachian age terrain (>3.7 Ga) the general assumption has been that they formed sometime during the end of the Noachian Period and possibly through the beginning of the Hesperian Period (Tanaka, 1986; Scott and Tanaka, 1986; Greeley and Guest, 1987; Carr, 1996; Hartmann and Neukum, 2001; Irwin et al., 2005; Fassett and Head, 2008). However, some studies suggest that valley network formation and prolonged fluvial activity extended into the Late Hesperian (Mangold et al., 2004; Quantin et al., 2005; Ansan and Mangold, 2006; Bouley et al., 2009) and possibly even the Amazonian (Scott and Dohm, 1992; Scott et al., 1995), although these latter studies focused on valley networks that occur in discrete, isolated areas, such as the flanks of volcanoes.

Part of the problem with assessing the temporal variations in valley network formation is that these features are very difficult to date using traditional crater counting techniques. The average width of a valley network is typically less than a few kilometers, so any crater with an appreciable size would actually destroy the valley network. Instead, some of the very first studies simply assumed that the valley networks were the same age as the

* Corresponding author. Address: IDES, UMR8148, Bat. 509, Université Paris XI, 91405 Orsay Cedex, France.
E-mail addresses: sylvain.bouley@u-psud.fr (S. Bouley), craddockb@si.edu (R.A. Craddock).

0019-1035/$ - see front matter © 2010 Elsevier Inc. All rights reserved.
doi:10.1016/j.icarus.2009.12.030

surrounding terrain (e.g., Carr and Clow, 1981). This assumption has been supported by mapping studies that show that valley networks are generally absent in units younger than Noachian in age; however, there are some observations that indicated valley networks incise some intercrater ridged plains that are generally Hesperian in age (Pieri, 1976; Tanaka, 1986; Carr, 1996; Bouley et al., 2009). Based on the 1:15M geologic maps of Mars (Scott and Tanaka, 1986; Greeley and Guest, 1987) Scott and Dohm (1992) suggested that 30% of valley networks may be younger than Noachian. Using larger scale maps, Carr (1995) suggested that this percentage was closer to ~8%. The advent of high-resolution imagery data from a suite of spacecraft in orbit around Mars can now be used to identify smaller diameter craters superposing valley networks and establish more reliable age estimates. We applied three distinct techniques to obtain the age of Parana Valles (Fig. 1), located between Margaritifer and Noachis Terra in a large basin that also includes Loire Valles and Erythraeum Chaos (Barnhart et al., 2009). This area was chosen because of the availability of high-resolution imagery and because it contains a relatively high density of valley networks. The age-dating methods we applied and assessed include the "buffered crater counting technique", which counts the number of craters that occur around the margin of the valley networks (Fassett and Head, 2008; Hoke and Hynek, 2008), another that we refer to as the "high resolution dating technique" counts smaller diameter craters that occur on the floors of the valley networks (Quantin and Craddock, 2008), and a third we refer to as the "basin technique", which counts the craters that occur in the drainage basins associated with the valley networks (e.g., Ansan and Mangold, 2006). Understanding the difference and limitations of these techniques will help us (1) establish when fluvial processes ceased on Mars, (2) assess the spatial and temporal variability of surface water on Mars, (3) determine which techniques are the most appropriate to age-dating valley networks and other features in support of mapping efforts, mission planning, and geologic analyses, and (4) as we demonstrate, allow us to assess some of the modification processes that took place subsequent to valley network formation.

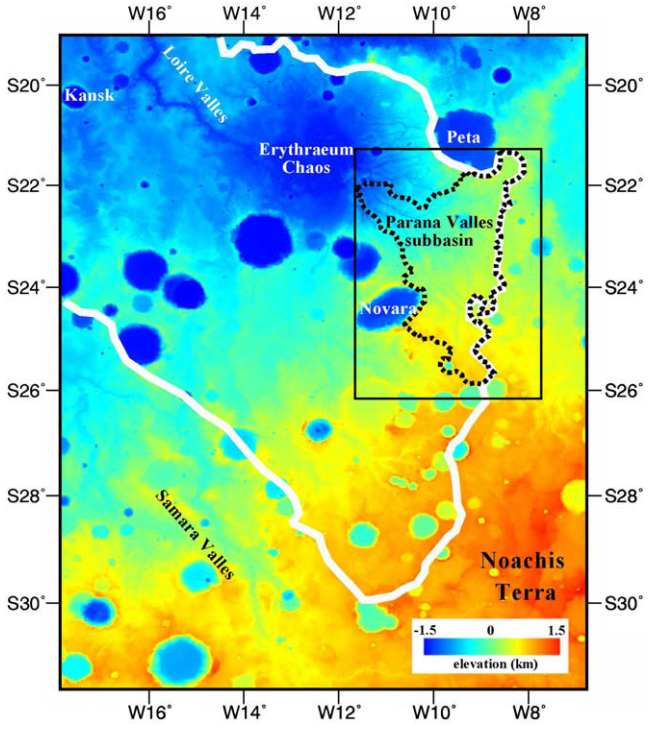

Fig. 1. MOLA topographic map for which most geographic features (e.g., terrae, impact craters, valleys) are labeled. The Loire/Parana Valles drainage basin, limited by the white line, determined by Barnhart et al. (2009). The Parana Valles sub-basin, limited by the black dash line, is determined with an automatic delineation of drainage basin perimeters software and MOLA data (460 m/pixel). The black box corresponds to the location of Figs. 2, 3, 11 and 14.

2. Background and approach

The first technique we applied in our study is often referred to as the "buffered crater counting technique" (Fassett and Head, 2008; Hoke and Hynek, 2008). Originally designed as a method for age-dating grabens on Mars (Tanaka, 1982; Wichman and Schultz, 1989; Nakimi and Solomon, 1994), the technique works equally well with other narrow, linear features, such as valley networks, providing image resolution is sufficient enough to identify smaller diameter craters. In this technique an area or « buffer » 1.5 times the impact crater diameter is established around the edges of a valley network. Craters that are counted include both those having their centers in the buffer and those intersecting the valley segment. The total surface area of the buffer is also calculated in order to normalize the counts and to determine the corresponding crater age-dates. Craters are excluded from the counts if they do not superpose the valley network (i.e. are integrated) or fall outside the buffer appropriate for the corresponding crater size. Fassett and Head (2008) determined the age-dates for 27 valley network systems in the highlands and found that typically most date to the Late Noachian, but several of the densest, most well-preserved systems date to the Early Hesperian, suggesting valley network formation may have continued for an extended period of time in several regions. Using this technique Hoke and Hynek (2008) found that 11 valley networks located in the martian highlands ceased formation at the end of the Late Noachian or during the Early Hesperian. Although their age estimates suggest that valley network formation did not cease earlier in martian history or extend significantly into the Hesperian, they suggest that valley networks did not form or cease formation at the same time. When comparing the age-dates from this technique, Hoke and Hynek (2008) noted several instances where their age-dates were different than those determined by Fassett and Head (2008).

The second technique, which we refer to as the "high resolution dating technique", involves counting impact craters on the floors of valley networks that are only a few tens to a few hundred meters in diameter. These counts are then normalized to the number of craters per 1 km^2 from 16 m to 256 km in diameter for comparison to the isochron diagram established by Hartmann (2005). Quantin and Craddock (2008) applied this technique to six valley networks that were located in the highlands and in other locations on Mars as well, including Alba Patera and Hecates Tholus. They found that in addition to the valley network episode that occurred in the highlands during the Noachian, there are flank of volcanoes where fluvial valleys formed during the Hesperian and Amazonian.

A third more traditional technique, which we refer to as the "basin technique", consists of counting craters within the whole valley network drainage basin (e.g., Ansan and Mangold, 2006). This technique typically provides the maximum age of the valley activity, and its reliability is improved when the density of valley networks is high so that almost all craters counted intersect valleys. To optimize this technique we used topography to define the drainage divides and contributing areas associated with valley network drainage basins and their smaller sub-basins. Such an approach is also helpful in determining if there were any temporal variations within the valley network systems themselves, and provides a maximum age-date for comparison with the other techniques.

In applying these techniques we also attempted to determine the consistency and limitations of each one to better understand

any possible temporal variations that may be associated with valley network formation. Age-dating techniques can only determine when fluvial activity ceased—not how long the fluvial activity may have been present. Indeed, fluvial processes continually modified all impact craters prior to and coeval to the valley activity, and the surface only became stable once these fluvial processes stopped (e.g., Craddock and Howard, 2002). Therefore, differences in age-dates may help us identify regions on Mars where fluvial activity may have persisted for longer periods of time or where fluvial activity was active most recently. Using the three techniques over the Parana Valles network, our results indicate that each technique is sensitive to crater preservation, and valley network ages are not only reflective of temporal variations in the cessation of fluvial activity, but also the amount and scale of subsequent modification that took place.

One critique of the fundamental counting crater method is the treatment of secondary impact craters. McEwen (2003) and McEwen et al. (2003) suggested that 75% of the craters superimposed on the floor of Athabasca Valles were secondary craters. Such a high population of secondary craters would obviously affect the age-dates. However, the lava plains in this region are very young (<100 Ma) and contain few primary craters, so the effects of secondary craters would profoundly affect the age-dates. However, in the Parana Valles region the surrounding terrains are Hesperian and/or Noachian in age. Although it is possible the area contains secondary impacts, the population of these craters would be small compared to the population of primary craters.

3. Data and methodology

We used three different sets of high-resolution images to obtain complete coverage of the Parana Valles drainage system (Fig. 2).

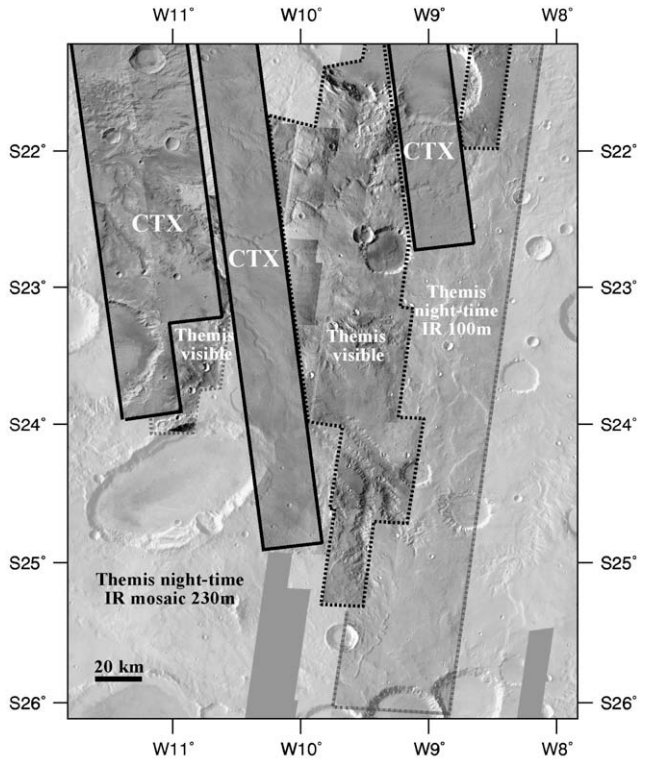

Fig. 2. Mosaic of four CTX images with a spatial resolution of 5 m/pixel, 18 THEMIS visible images (17–35 m/pixel), 3 THEMIS day-time IR images (100 m/pixel) and THEMIS day-time IR mosaic (230 m/pixel) in the background. This mosaic covers Parana Valles sub-basin.

We mosaicked four images acquired by the Context Camera (CTX) of Mars Reconnaissance Orbiter (Malin et al., 2007) that have a spatial resolution of 5 m/pixel (images P08_004131_1565, P14_006689_1588, P15_006755_1582, P16_007467_1578). However, the available CTX images do not cover the entire Parana Valles drainage system, so we included additional data from the Thermal Emission Imaging System (THEMIS) (Christensen et al., 2003) day-time infrared (IR) and visible images (Fig. 2). We used 18 visible THEMIS images with a spatial resolution of 19 m/pixel as well as 3 THEMIS day-time infrared having a spatial resolution of 100 m/pixel to aid in the geologic interpretations. Combined, the CTX images and visible THEMIS images covered the entire Parana Valles drainage system with a minimum image resolution of >20 m/pixel for use in our analyses. These data allowed us to precisely and manually map the Parana Valles drainage system and to count craters with diameters of 125 m and larger. We also used a mosaic of THEMIS day-time infrared image with a resolution of 230 m/pixel to provide a regional context of the Parana Valles drainage system as well as a THEMIS night-time mosaic to identify differences in the physical properties of the surface materials within Parana Valles and the surrounding area.

A digital elevation model (DEM) using 1/128 gridded Mars Orbiter Laser Altimeter (MOLA) (Smith et al., 1999) data was used to extract the drainage divides associated with Parana Valles and its sub-basins as described below. The MOLA DEM has a spatial resolution of ~460 m/pixel and a vertical accuracy of ~1 m (Fig. 3). All data were ortho-rectified to the martian sphere with an axis of 3396 km and placed into a sinusoidal projection centered at 10°W longitude. Geographic coordinates followed the martian standard coordinate system with planetocentric latitudes and east longitudes (Duxbury et al., 2002).

A variety of algorithms has been written to extract watershed information from DEMs in support of terrestrial studies (Palacios-Velez and Cuevas-Renaud, 1986; Martz and Gabrecht, 1992; Zhang and Montgomery, 1994; Tarboton, 1997). The original algorithm is called the D8 flow model, but there have been several advances of this model through time that allow better computation of divergent flows on hillslope, such as the D–∞ model (Tarboton, 1997) and the Mass Flux Method (Costa-Cabral and Burges, 1994), as well as flow over flat terrain (Garbrecht and Martz, 1997). For simplicity, we only describe the D8 flow model, which determines the flow direction from every grid cell in a DEM by calculating the steepest downhill slope from a grid cell to the eight surrounding grid cells. Cells with undefined flow directions are resolved iteratively by assigning them the lowest values from one of the neighboring cells with defined flow directions. The results are stored as a grid file with the same dimensions as the DEM. The values recorded in each grid cell are representative of the flow direction from that particular cell (e.g., 1 is NE, 2 is E, 4 is SE, and so on).

As the flow path is traced from one grid cell to the next it eventually encounters the flow path from adjacent grid cells. These separable flow paths represent unbranched tributaries referred to as first-order streams. There are three different methods of ordering streams after they have joined. Horton's (1945) original method assigns an order for each stream based on its relative importance in the network while Strahler's (1952) method assigns an order to each segment. Strahler's system is less cumbersome in that two first-order streams come together to form a second order stream, two second order streams join to form a third order stream, and so on. Shreve Magnitude (Shreve, 1967) assigns an order to each segment based on the number of upstream links formed by tributaries. To better compare with previous studies the Horton stream ordering system is used in this manuscript.

The total area flowing into each cell is defined as the contributing area, and by adding these values for every cell along the flow path of a particular stream it is possible to calculate the drainage

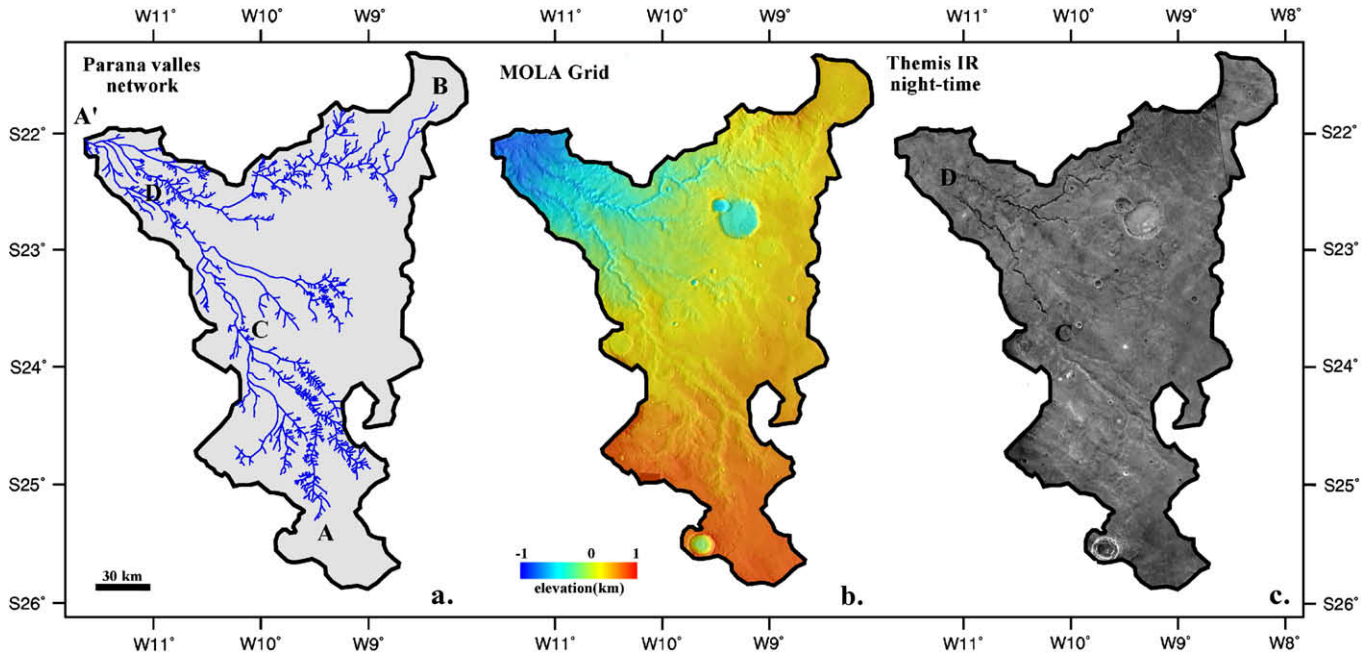

Fig. 3. (a) The Parana Valles drainage basin, represented in gray, determined with an automatic delineation of drainage basin perimeters software and MOLA data, at 460 m/pixel. Blue lines represent observed fluvial valleys in the sub-basin. (b) Parana Valles sub-basin with a MOLA topographic map on the region of Parana Valles with a spatial resolution of 460 m/pixel. (c) Parana Valles sub-basin with THEMIS IR night-time mosaic (230 m/pixel). We noted the difference of signal between the interior of valleys downstream and upstream.

area for that stream. Because such drainage areas fit into the larger drainage basin, they are commonly referred to as sub-basins and are denoted by the largest order stream that they support. By integrating the contributing areas for the entire network, it is possible to determine the surface area for the drainage basin as well as its boundaries or drainage divides.

4. Parana Valles network characteristics

Parana Valles is located between Margaritifer and Noachis Terra in a large basin that also includes Loire Valles and Erythraeum Chaos (Barnhart et al., 2009). Parana Valles was chosen as a site for evaluating the different age-dating techniques because of the good coverage high-resolution imagery and the high density of valleys. A description of the network is required before evaluating the crater counts.

4.1. Drainage basin morphometry

The drainage basin and divides were extracted from a digital elevation model constructed from 1/128 MOLA and compared to the image mosaics (Fig. 3). The Parana Valles basin is a NW–SE elongated catchment with a 280 km major axis, covering an area equal to 26,652 km^2 (Fig. 3). The Parana basin contains two main tributaries starting at A and B shown in Fig. 3 and joining each other at point A′.

The segment AA′ is a NW–SE elongated valley with a maximum length of 255 km. This segment has several headwall scarps located inside Noachis Terra south of the Parana basin and southeast of Novara crater. These valley heads are at the headwaters of a branching network that incises a smooth plateau located above 500 m elevation. The different tributaries join each other at point C located at 250 m elevation and continue until point A′.

The segment BA′ is an E–W elongated valley with a length of 240 km. This segment includes a main valley with a unique headwall scarp located at point B at 350 m elevation. This valley head is located in a circular smooth plateau, which could be the remnant of an impact crater. Many small tributaries intersect with the main trunk channel along the path of this segment.

Parana basin debouches into the 300 km diameter Erythraeum Chaos (point A′), which was interpreted as a degraded paleolake (Grant, 1987; Grant and Parker, 2002; Howard et al., 2005). Sedimentary deposits located on the floor of this basin may have been emplaced by Parana Valles (Goldspiel and Squyres, 1991; Grant and Parker, 2002).

Our measurements show that Parana Valles is a sixth order stream using the Horton system (Horton, 1945) with a manually mapped total length of all the drainage segments of 3586 km (Fig. 3a), resulting in a total drainage density of 0.13 km^{-1}. This drainage density is consistent with the density of 0.14 km^{-1} determined by Hoke and Hynek (2008) using THEMIS IR night images.

4.2. Valley morphology

From spacecraft images, individual valleys of the Parana basin show three different morphologies that can be distinguished from east to west at distinct elevations (Fig. 4). First, to the east near the divide within the first hundred kilometers next to the valley head A, between 200 m and 600 m elevation, cross sectional profiles show that valleys are generally rectangular for the main tributaries. The widths of the valleys range from 8 km near the source to 2 km further downstream (Fig. 5). Imagery data show that the smaller contributing valleys in this area have a classic V-shaped profile with amphitheatre shaped headwalls <100 m in width (Fig. 6).

Comparison of valley shapes with the topographic data shows a correlation between the valley width and the regional slope (Fig. 5). Indeed, the slope of the channel segment from A to C, is ~0.3%, where the width is between 2.5 and 8 km. Near point C, however, the slope becomes steeper at ~0.7%, and the width of valleys becomes narrower at ~2 km even when the valleys show a rectangular cross section. In this second section of the network,

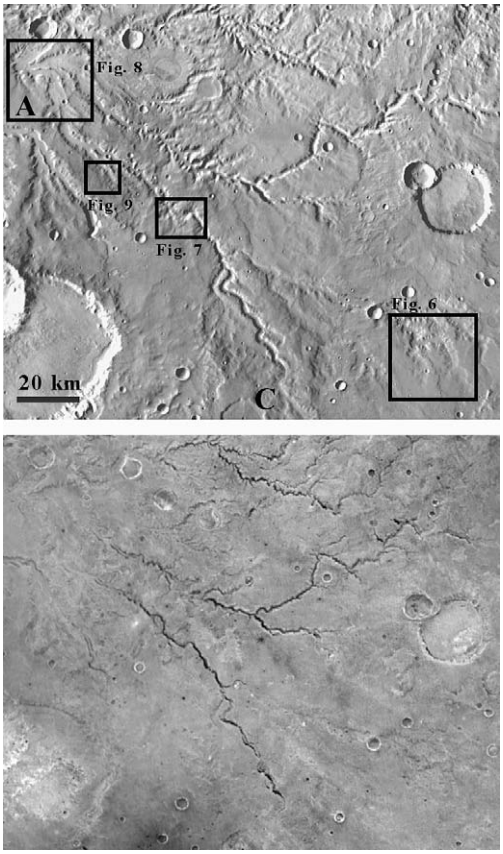

Fig. 4. (Top) THEMIS IR day-time view (230 m/pixel) of the downstream Parana Valles sub-basin. (Bottom) THEMIS IR night-time view of the downstream Parana Valles sub-basin showing the high thermal signal inside Parana valleys.

between C (200 m elevation) and D (−700 m elevation), of the number of tributaries are also less frequent. In addition, visible imagery shows the presence of small dunes on the floor of the main tributary, indicating that some eolian deposition or reworking has occurred (Fig. 7). These landforms show a dark thermic signal on THEMIS night-time IR images (Fig. 4).

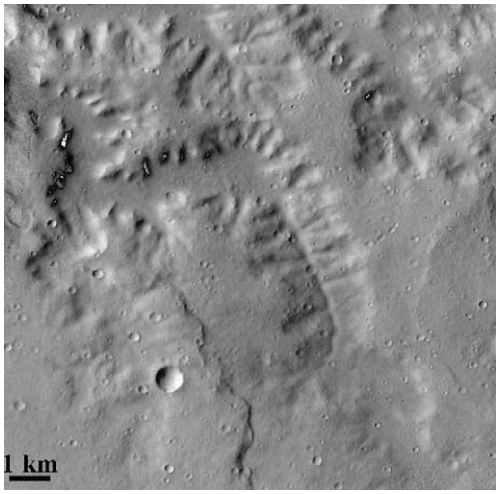

Fig. 6. THEMIS visible close-up (23°27′S; 9°24′W) of heads and valleys with a resolution of 17 m/pixel; position of this close-up indicated in Fig. 4.

A third type of valley morphology is observed closer to the Parana outlet, between D (−700 m elevation) and A′ (−1100 m elevation). Fig. 8 shows that these valleys are generally wider (2–4 km) than the valley in the segment CD, and the widths vary considerable along the length of the valleys unlike the valley networks further upstream. Several filled craters with a maximum diameter of 200 m (Fig. 8) are observed suggesting that substantial deposition has taken place. A small 12-km long and 250-m wide channel incised the bottom of the valley, indicating that last stage of Parana Valles fluvial activity is still preserved on the valley floor. This implies that any subsequent eolian filling was minimal, and that the sediments on the floor of the valley were probably emplaced during the primary formation of the valley network. This is supported by THEMIS night-time images that show that this part of the basin contains thermally brighter (warm at night) material that is inconsistent with dune deposits seen elsewhere in the valley.

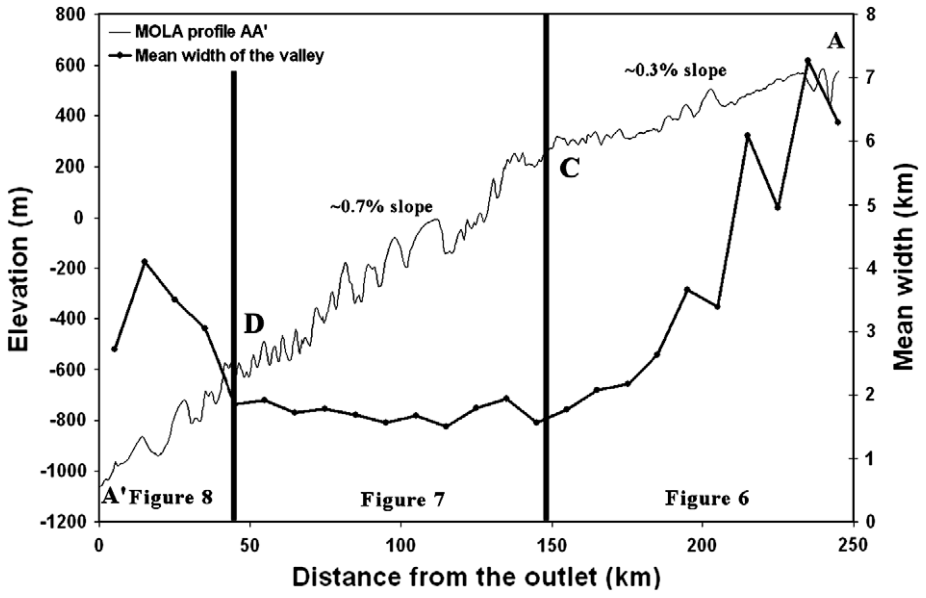

Fig. 5. MOLA profile AA′ showing two different slopes on the path of the valley (thin line). Variation of mean width given for each 10 km segment along the path AA′ (bold line).

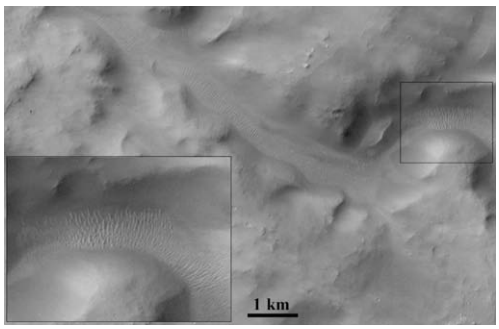

Fig. 7. CTX close-up (22°48′S; 10°46′W) of valley with a resolution of 5 m/pixel showing eolian dunes inside. Position of this close-up indicated in Fig. 4.

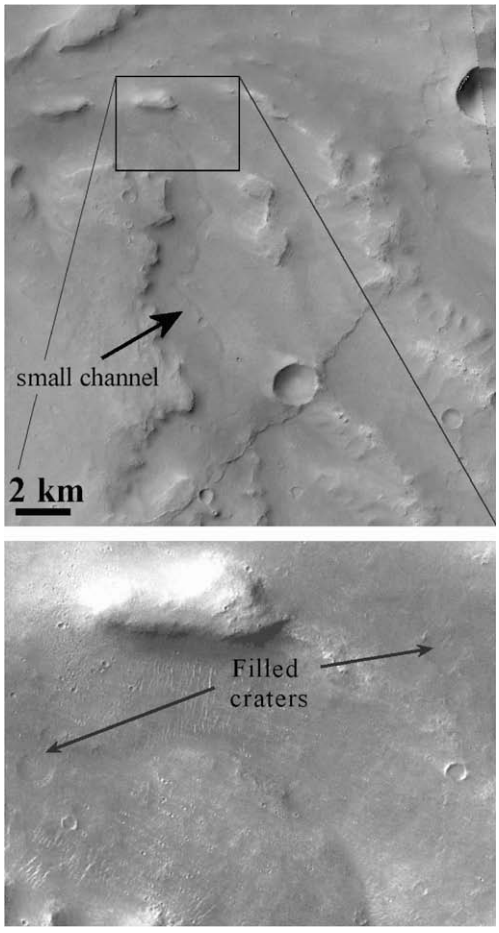

Fig. 8. CTX close-up (22°09′S; 11°24′W) of outlet of Parana Valles sub-basin with a resolution of 5 m/pixel showing resurfacing of the interior of valleys. We observe some filled craters and a small channel on the floor of the valley. Position of this close-up indicated in Fig. 4.

4.3. Incised terrains morphology

The terrains that were incised by valley networks in this region were observed to have two distinct morphologies. Fig. 6 shows that upstream valleys (>200 m elevation) are located in smooth terrains that contain many small impact craters that are close to saturation. These terrains are not degraded and appear to have no superficial erosion. In contrast, narrow valleys downstream are located inside rougher terrains that contain only a few small impact craters, some larger craters, and isolated mesas that have been heavily modified (Fig. 9). This terrains appears to have been affected by intense

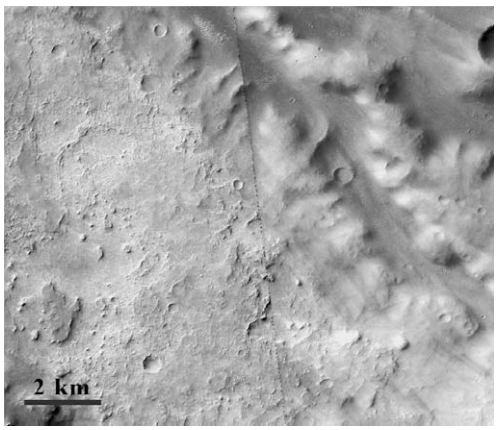

Fig. 9. CTX close-up (22°35′S; 11°12′W) of degraded downstream terrains. We note the presence of mesas and modified craters on these incised terrains. Position of this close-up indicated in Fig. 4.

superficial fluvial erosion as indicated by the scabby texture of the surface. NW–SW oriented windstreaks suggest that eolian processes may be ongoing within these terrains. The difference in the style of degradation between the downward and upward part of plateau may reflect differences in lithology.

5. Age-dating results

Because high-resolution images were not available for the entire Parana Valles basin, it was not possible to count all craters down to 125 m in diameter, which would have allowed us to compare the statistics of smaller diameter craters populations between all the different techniques. To determine the absolute ages, we plotted incremental crater densities using the Hartmann diagram (Hartmann, 2005) (Table 1). We also measured $N(1)$ values (density of cumulative number of craters of more than 1 km) to determine the formation period of the valleys using established crater density boundaries (Tanaka, 1986). The $N(1)$ values also allowed us to compare our results to results presented by Fassett and Head (2008) and Hoke and Hynek (2008).

Fig. 10 shows the incremental crater densities as determined by the three techniques. Results show that the buffer technique (red curve) yields a Late Noachian age. The high resolution dating technique (green curve) yields a Late Noachian to Early Hesperian age. The basin technique (blue curve) yields an Early Hesperian age, and the corresponding incremental ages parallel to the 3.5 Gyr iso-

Table 1
$N(0.125)$, $N(0.353)$ and $N(1)$ and uncertainties calculated for the three different dating techniques applied to the whole Parana Valles sub-basin and determined age period. HR: high resolution dating technique; basins: basin dating technique; buffer: buffer dating technique. $N(X)$ gives the number of crater up to X km. Bold font gives the cumulative crater density for craters up to X km. Uncertainties represent a 1-σ interval of $\pm\sqrt{N(X)}$/Sup (Sup: sub-basin area in km^2). LN: Late Noachian; EH: Early Hesperian.

Method	HR	Basins	Buffer
Sup (km^2)	2194	21,725	4096
$N(0.12)$	1612	–	–
$N(0.12)$ craters/km^2	**0.735**	–	–
±	0.018	–	–
$N(0.35)$	206	1825	–
$N(0.35)$ craters/km^2	**0.094**	**0.084**	–
±	0.0065	0.0020	–
$N(1)$	10	91	26
$N(1)$ craters/km^2	**0.0046**	**0.0042**	**0.0063**
±	0.0014	0.0004	0.0012
Age period	**LN to EH**	**EH**	**LN**

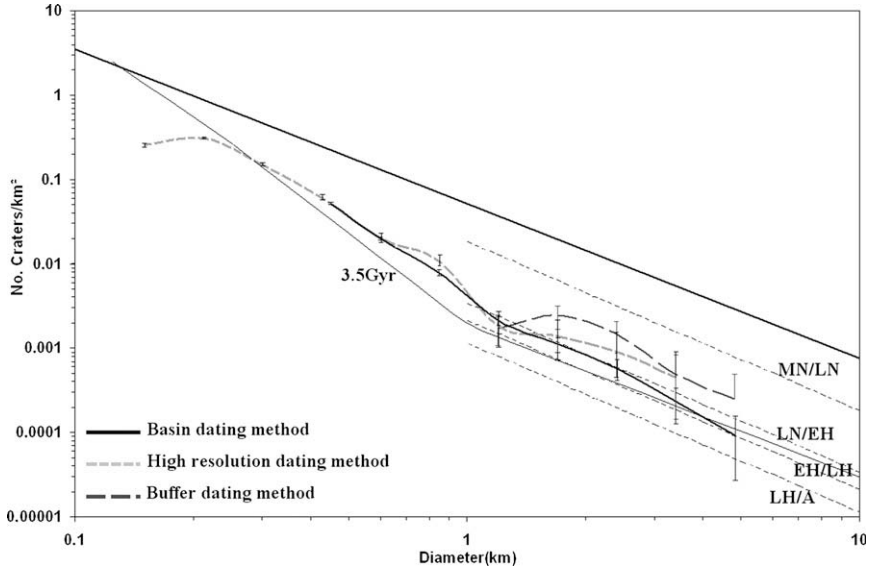

Fig. 10. The incremental crater densities of the Parana Valles sub-basin using three different techniques are plotted. In bold, the basin dating technique; in short dashed, the high resolution dating technique and in long dashed, the buffer dating technique. The −2 power laws (Hartmann, 2005) given by dashed lines mark the boundaries between, from lower to upper, the Late Hesperian–Amazonian (LH–A), Late Noachian–Early Hesperian (LN–EH), Middle Noachian–Late Noachian (MN–LN). Error bars represent a 1-σ interval of $\pm\sqrt{nj}/Aj$ (nj: number of crater for one interval; Aj: studied area in km^2). The thin solid black line is the 3.5 Gyr boundary. Hartmann Laws are valid for crater >1 km and do not propagate out linearly. They should theoretically be parallel to the 3.5 Gyr isochron.

chron. The cumulative $N(1)$ values presented in Table 1 are consistent with ages determined from the Hartmann diagram for craters >500 m.

Our results show that the basin technique provides a younger age than the two other techniques. Because we have only counted the fresh impact craters that have not been modified, we would argue that these populations of craters record the time when fluvial processes ceased in the surrounding highlands and the contributing area. This age would be the same as the valley networks if crater modification and valley network formation were caused by the same fluvial process. The age derived from the basin technique would be older than valley networks if the surrounding highlands were unaffected by fluvial processes as valley formation was occurring. Potentially the age derived from the basin technique could be younger than the valley networks if somehow craters were preferentially eroded from the surrounding highlands while leaving the valley networks and local craters unaffected. This seems unlikely, however. The valley networks are only a few kilometers across, yet the crater populations derived from the basin technique are up to 5 km in diameter. It is ad hoc to assume that a process capable of eradicating a 5-km crater would not affect the larger valley networks in this area.

The younger age observed by the basin technique, may simply be a matter of statistic and the number of craters counted. There were 91 craters >1 km used in the basin technique while the buffered technique used only 26 craters >1 km in diameter. Consequently, the error bars are much larger for the buffer technique, and we argue that the accuracy of the basin technique is simply better.

The small scale valley dating technique includes a large population of craters with diameters of 125 m (>1000 craters, Table 1). However, the population becomes statically unreliable at larger diameters approaching 1 km; the number of craters >1 km is only 10, which limits the usefulness of comparing age-dates between the different techniques at this crater diameter. Here too the apparent older age at crater diameters >1 km may be the result of the small sampling size. This technique is also more sensitive to the degradation of small craters. For example, the progressive shift of crater densities below 250 m may be due to modification such as the eolian blanketing that is apparent in the image data (Fig. 7). Thus, this technique should be applied only to crater diameters large enough to have not been affected by modification processes, yet where the population is large enough to be statistically significant. The similarity of age between the basin technique and the small scale valley dating for crater diameters in the range of 350–500 m in Fig. 10 suggests that this crater size is the most appropriate for age-dating for Parana Valles while providing an adequate population size. It is important to note, however, that these parameters may change from one region to another due to variations in crater preservation and the size of the counting area.

6. Spatial variations in crater densities

We studied variations in crater densities inside the Parana Valles basin both at the scale of tributaries and within the trunk channel using the high-resolution technique and at the scale of the Parana sub-basins using the basin technique. The buffered crater counting technique does not lend itself to being applied easily to smaller areas within the drainage basin or the valley network system.

6.1. Age variations within valleys

The main trunk channel and tributaries of Parana Valles was divided into 10 km long segments to determine if there was any local variation in crater densities within the floors of the valley networks. For each segment we counted both fresh and modified craters >125 m in diameter on the floor of the valley and then estimated $N_{\mathrm{fresh}}(0.125)$ and $N_{\mathrm{all}}(0.125)$, which are the cumulative numbers of these craters >125 m/km. This analysis was possible because of the high resolution of the available images, which allowed us to identify the crater populations necessary for obtaining a statistical significant sample.

Fig. 11 shows the variations in fresh crater $N(0.125)$ densities on the floor of several valleys of the Parana Valles system. Each color corresponds to different crater densities within different valley network segments. We found that $N(0.125)$ values are not

homogeneous along the different tributaries and ages can be divided into two distinct groups. The first group includes valley network segments located down channel that typically have low $N(0.125)$ crater densities (<0.6 craters/km^2). These segments are all located at MOLA elevations <200 m. The second group includes segments that are located further upstream with densities >0.8 craters/km^2, which contain 2–5 times more craters than segments located downstream.

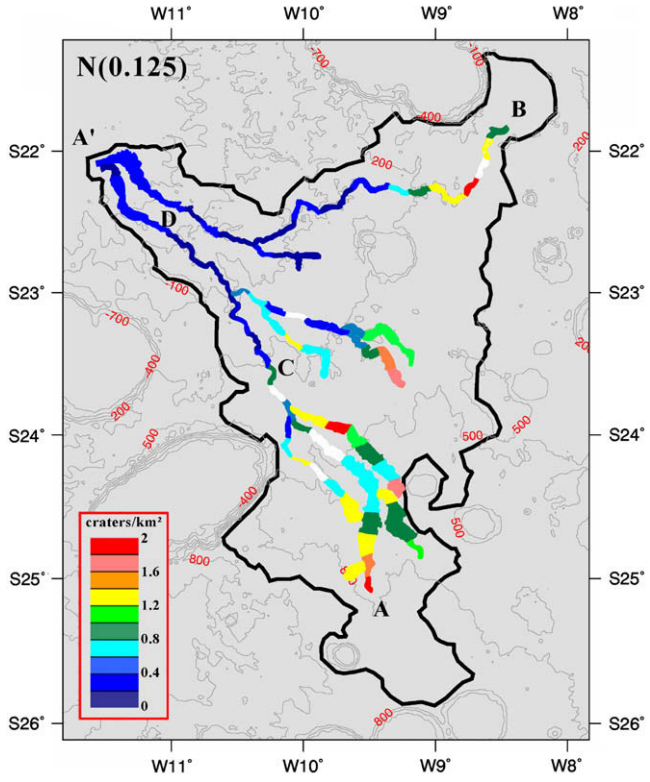

Fig. 11. Variation of crater density $N(0.125)$ (number of craters larger than 125 m/km^2) calculated for the bottom of valley's segments of 10 km in length of Parana Valles. Crater density was determined by the small scale valley technique dating. White segments correspond to segments with no data because of low resolution images. We noted the important difference of crater density between the interior of valley upstream and downstream.

One possible explanation for these striking differences in ages may be due to an eolian mantling that buried some of the craters on the valley floors. Indeed, several locations where lower crater densities were found correlate with thermally dark area and where small dunes on the valley floors were seen. However, the last 50 km segment (segment D–A′) also has low crater densities, yet there are no obvious eolian landforms or thermally dark material in visible and night-time IR imagery (Fig. 4). However, it is apparent that this area was also resurfaced as evidenced by partially buried craters with maximum diameters of 200 m.

To better understand the decrease in craters density near the valley network outlet we plotted the variation of $N_{fresh}(0.125)$, cumulative number of fresh craters larger than 125 m, and $N_{all}(0.125)$, cumulative number of fresh and modified craters larger than 125 m, along segment A–A′ (Fig. 12). Within segment CA′, the value of $N_{fresh}(0.125)$ is almost constant (~0.2 ± 0.2 craters/km^2). The $N_{all}(0.125)$ values are similar within segment C–D, but these values increase within segment D–A′. This may indicate that the mantling did not bury all craters in this valley segment. Furthermore, Fig. 5 shows that the valley is wider along segment D–A′, with a local channel present on the valley floor; eolian deposits are also more obvious within segment C–D. These observations suggest that valleys close to the outlet were filled and partially resurfaced before the last stage of fluvial activity. Moreover, late eolian deposits formed after fluvial activity within Parana Valles ceased and preferentially concentrated where the valley networks are narrower.

In the upstream area, $N(0.125)$ is higher than in the lower sections with values ~2 craters/km^2 in some segments close to valley heads (Fig. 11). Values of $N_{fresh}(0.125)$ and $N_{all}(0.125)$ are equal along the A–C segment (Fig. 12). The channel segments in this area also appear to be free of eolian deposits, too. However, the crater statistics suggest that some sort of resurfacing occurred, such as a sedimentary filling. Indeed, if there was no resurfacing, $N_{all}(0.125)$ values should be constant along the floor of the valley, but data shows a downstream decrease of this density, from 0.6 to 2 craters/km^2 (Fig. 12). This difference can be explained by shallow resurfacing that occurred in the upstream valleys that increased in thickness down channel.

Fig. 13a provides some additional evidence supporting these interpretations. This figure shows that ages deduced from crater

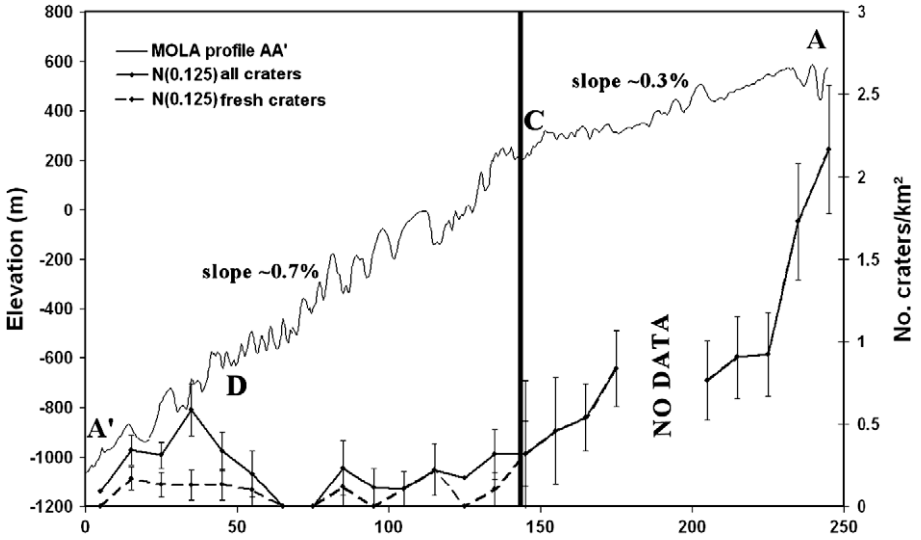

Fig. 12. MOLA profile AA′ and variation of $N(0.125)$ fresh craters and $N(0.125)$ all craters (number of crater up to 125 m/km^2) calculated for the bottom along of the valley AA′.

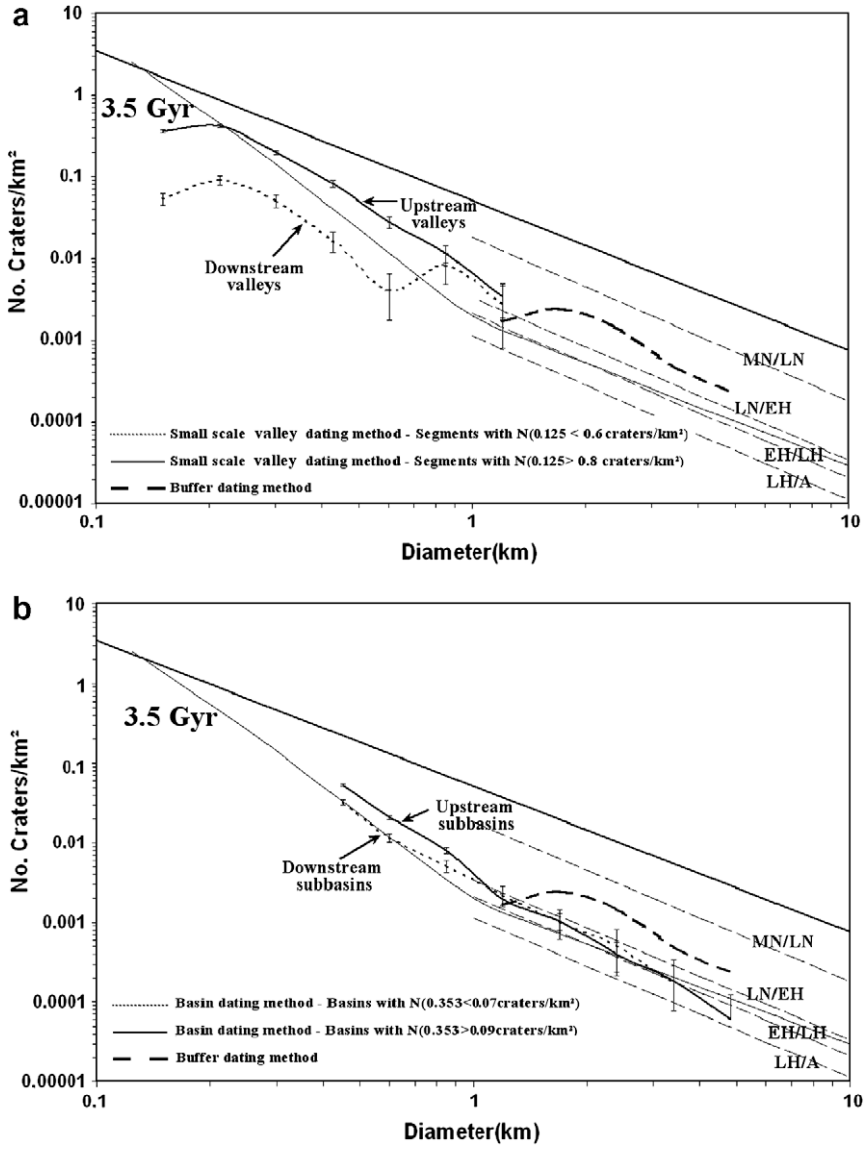

Fig. 13. (a) The incremental crater densities of the interior of valleys. The solid line gives the retention age of valley's with $N(0.125) > 0.8$ crater/km^2 corresponding to upstream valley's segments. The dotted line gives the retention age of sub-basins with $N(0.353) < 0.6$ crater/km^2 corresponding to downstream valley's segments. (b) The incremental crater densities of the 18 Parana Valles sub-basin. The solid line gives the retention age of sub-basins with $N(0.353) > 0.09$ crater/km^2 corresponding to upstream sub-basins. The dotted line gives the retention age of sub-basins with $N(0.353) < 0.07$ crater/km^2 corresponding to downstream sub-basins. The -2 power laws (Hartmann, 2005) given by dashed lines mark the boundaries between, from lower to upper, the Late Hesperian–Amazonian (LH–A), Late Noachian–Early Hesperian (LN–EH), Middle Noachian–Late Noachian (MN–LN). Error bars represent a 1-σ interval of $\pm\sqrt{nj}/Aj$ (nj: number of crater for one interval; Aj: studied area in km^2). The thin solid black line is the 3.5 Gyr boundary. The dashed line corresponds to the incremental densities of the Parana Valles sub-basin using buffer dating technique. Hartmann Laws are valid for crater >1 km and do not propagate out linearly. They should theoretically be parallel to the 3.5 Gyr isochron.

density are not the same for the upstream (bold curve) and downstream (dotted curve) valley floors. The bold curve shows that upstream valleys floors have an early Hesperian age. The dotted curve with a Late Hesperian/Early Amazonian age shows that downstream valley floors were resurfaced creating a deficit of craters <700 m in diameter, or ~0.8 craters/km^2 for craters with diameters between 125 and 700 m. These observations imply that resurfacing of the valley networks was more intense downstream than upstream. As mentioned previously, the filling of downstream valleys has two possible origins: (1) resurfacing by fluvial sediments emplaced during late-stage Parana Valles activity and (2) later resurfacing by eolian deposits that preferentially seemed to have filled narrower sections of the valley networks. It should also be noted that the amount or intensity of resurfacing within the valley networks becomes negligible closer to the headwater areas. There are many craters <700 m diameter apparent in these upper reaches. The apparent Early Amazonian/Late Hesperian ages found for craters between 125 and 700 m in diameter (Fig. 13a) in the lower segments appears to be simply an artifact of late or subsequent resurfacing within the valley networks. This implies that the high resolution age-dating technique is valuable for deciphering the complex geologic history of a valley network system, but caution should be used when applying these ages to understanding the cessation of fluvial activity within the system itself. The resurfacing may not always be fluvial, and other geologic analyses are necessary to place the crater ages into context.

6.2. Thickness of eolian or fluvial blanketing inside valleys

Burial and erosion are the two relevant processes which are able to explain the lack of craters <700 m in the lower segments of Parana Valles. Assuming burial by eolian or fluvial deposits

was the process primarily responsible for eradicating craters, it is possible to estimate the minimum thickness of these deposits by estimating the rim height (h_r) of the smallest, unaffected craters, which can be estimated from the incremental curve (Mangold et al., 2009). For craters with diameters <7 km Garvin (2002) showed that:

$$h_r = 0.07D^{0.52} \quad (1)$$

where h_r is the rim height and D is the crater diameter. To bury craters <700 m, which is the largest bin to be affected by the filling, the thickness of the resurfacing materials would have to be ~60 m.

Closer to the valley mouth at A′, we observed some partially buried craters with a maximum diameter of 200 m (Fig. 8). From Eq. (1), the calculated thickness of the sediments infilling this crater is ~30 m. However, this is not the total thickness of the deposit in this area as evidenced by the total crater population. The fact that these craters are only partially buried indicates that the total thickness of 60 m took long enough time to be emplaced as to allow some impact cratering to occur.

6.3. Age variations within the sub-basins

Parana Valles can be divided into 18 different sub-basins with Horton orders of 3–6 and surface areas ranging from 332 to 2657 km^2 (Table 2). For each sub-basin we measured $N(0.353)$, which is the cumulative numbers of crater >353 m in diameter/km^2, with 1-σ error (Table 2). The goal of the $N(0.353)$ crater count was not to determine an absolute age of any of the sub-basins but rather to compare relative ages between the different sub-basins. Basically, $N(0.353)$ ages were the smallest crater populations visible given the available image resolution of the entire region. Craters with this diameter have populations with sufficient sampling sizes as to provide good results, although craters with diameters >125 m would have been better for comparison with our other results.

The fresh crater densities ($N(0.353)$) in the 18 different sub-basins are not homogeneous within the Parana Valles catchment (Fig. 14). Table 2 presents the surface area (in km^2) for each sub-basin, the corresponding $N(0.353)$ values, the derived uncertainties and the maximum Horton order. Two different groups of values can be distinguished. Most sub-basins located upstream have values >0.08 craters/km^2 with the exception of sub-basins numbers 3 and 11. Three downstream sub-basins, numbers 1, 2 and 10, have $N(0.353) < 0.06$ crater/km^2. The observed variations in $N(0.353)$ within the Parana Valles sub-basins can be explained by a resurfacing process that was more intense downstream than upstream, similar to what was observed within the valley network segments.

The Parana Valles system was formed by the erosion of a plateau located above 500 m elevation. This plateau is incised in some places, but the crater retention age for the upstream sub-basins ($N(0.353) > 0.08$ craters/km^2) is close to the formation age of the plateau. Absolute ages can be determined by the martian impact cratering chronology curve as determined by Hartmann (2005) as shown in the bold curve presented in Fig. 13b. The crater populations are parallel to the 3.5 Gyr isochron, and are thus at the Late Noachian–Early Hesperian age boundary. For craters >1.4 km, error bars are larger, but the absolute ages are also Late Noachian to Hesperian.

The dotted line in Fig. 13b shows that the sub-basins located downstream ($N(0.353) < 0.06$ craters/km^2) have a younger retention age for craters of 353 m to 1 km, but a similar age for craters >1 km. This variation of crater density indicates that sub-basins located downstream were also resurfaced during the Early to Late Hesperian. Terrains in this area show erosional landforms on plateaus surface (Fig. 9). The observed resurfacing with younger retention ages can be explained by eolian or fluvial activity within the downstream sub-basins that was active during the Early to Late Hesperian. From the ages of the sub-basins, it appears that Parana Valles formed during the Early Hesperian, with its latest activity occurring during the Late Hesperian.

Table 2
$N(0.353)$ and uncertainties calculated for the 18 sub-basins with basin dating technique. No. sub-basin corresponds to the number of sub-basin in Fig. 6. N crater gives the number of crater up to 353 m. Uncertainties represent a 1-σ interval of $\pm\sqrt{N}$ crater/area (area: sub-basin area in km^2). For each sub-basin is indicated the maximal Horton order of the network.

No. sub-basin	Area (km^2)	N crater	$N(0.353)$ (N crater/km^2)	±	Maxi. order
1	1675	90	0.054	0.006	6
2	1116	70	0.063	0.007	5
3	539	43	0.080	0.012	3
4	1127	103	0.091	0.009	4
5	1753	158	0.090	0.007	3
6	911	91	0.100	0.010	3
7	292	29	0.099	0.018	3
8	335	32	0.096	0.017	3
9	517	48	0.093	0.013	3
10	2716	150	0.055	0.005	6
11	797	67	0.084	0.010	4
12	1158	115	0.099	0.009	3
13	2370	213	0.090	0.006	3
14	797	72	0.090	0.011	3
15	1664	171	0.103	0.008	3
16	2438	222	0.091	0.006	4
17	677	74	0.109	0.013	3
18	843	77	0.091	0.010	3

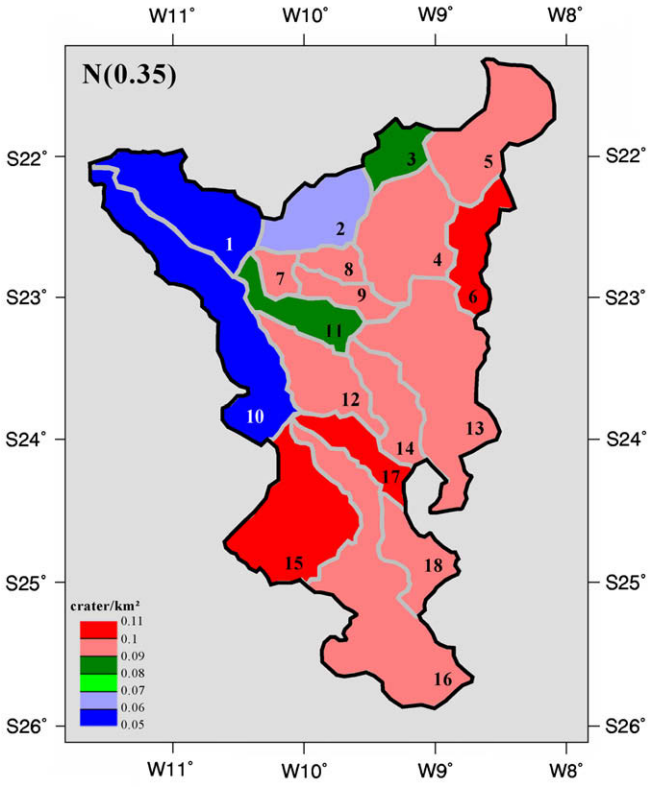

Fig. 14. Variation of crater density $N(0.35)$ (number of crater up to 353 m/km^2) inside 18 sub-basins of Parana Valles sub-basin. Details of crater density are given for each number of sub-basin in Table 2. Crater density was determined by the basin technique dating. We noted the important difference of crater density between sub-basins upstream and downstream.

7. Discussion

Our results validate the reliability of all the proposed age-dating techniques and demonstrate that crater populations can be used (1) to determine the relative ages of valley networks, (2) to determine if subsequent resurfacing and surface modification took place and (3) to assess the spatial variation in intensity of these processes. Fig. 15 summarizes the different observations made for the interior of the valley networks. Previously, we showed that thickness of deposits filling valleys is minimum close to the source with a maximum thickness of ~60 m near the outlet. We showed also that craters may have formed as this deposit was being emplaced, suggesting that deposition occurred over an extended amount of time.

There are several possible origins for the downstream deposits identified in the Parana Valles drainage basin. If the thickness increases progressively, Parana Valles fluvial activity may have transported sediments from upstream to downstream. However, we have seen previously that downstream sub-basins were eroded coevally with the deposition of these downstream deposits. It is possible that sediments eroded from the surrounding sub-basin terrain may have infilled the valley. However, incision by small channel in the floor of the valley indicates that the downstream deposits were emplaced prior to the cessation of fluvial activity within Parana Valles. It may be that these deposits consist of both eolian and fluvial sediments, which were emplaced during the Early Hesperian that progressively filled the valleys. Subsequently, eolian processes created dunes within portions of the valleys. Indeed the resurfacing within the downstream valleys ceased more recently than within the downstream sub-basins (Early Amazonian versus Late to Early Hesperian, as shown in Fig. 15, profile 2). It is likely that the valleys are currently acting as traps for windblown sand and dust.

It is difficult to determine why the erosion of the sub-basins was more pronounced downstream than upstream. As mentioned before, the morphology of the downstream and upstream valleys are different, which can be the result of a difference of lithology between the two terrains. Lithologic differences could also explain why the downstream terrains appear more easily eroded than the upstream terrains, too (Barnhart et al., 2009). It is also possible that overflow and fluvial erosion was more pronounced in the downstream sub-basins. Unfortunately the geologic evidence does not allow us to reliably determine the relative importance of these two different processes.

8. Conclusions

We tested the reliability and applicability of three different valley network age-dating techniques by applying them to the Parana Valles drainage system. All of the techniques have their positive attributes and can be used to determine the age of Parana Valles, the distribution of sedimentary materials within the valley and catchment, and the extent of resurfacing events that occurred during and after valley network formation.

8.1. Age-dating methods

Our study demonstrates that:

(1) The buffer crater counting technique is more reliable in locations where the counting area is large. This technique can be applied on older valley networks because of the relatively larger population of craters, but this technique may miss younger reactivation or resurfacing because it requires analyzing the valley network system in its entirety. In our test, we found that the age for the valley networks determined by this technique was older than the surrounding highlands, probably because of the small number of craters that formed the basis for this age-date. Fassett and Head (2008) also applied the buffered crater counting technique and derived an age for Parana Valles that was more comparable to our results, but they used a much larger counting surface that included Loire Vallis that resulted in a population of 84 craters 2–32 km in diameter. Thus, the reliability of the buffered crater counting technique would seem to decrease when it is applied to smaller drainage basins and smaller surfaces. For the same reasons, this technique is not useful for extracting age variations within a given valley network drainage system. In the case of valley networks that are Hesperian or Amazonian in age there are not enough smaller diameter craters (>1 km) to determine the absolute ages with any given certainty using the buffered crater counting technique. Indeed, because of the small sampling sizes, the ages derived by Fassett and Head (2008) typically do have large uncertainties.

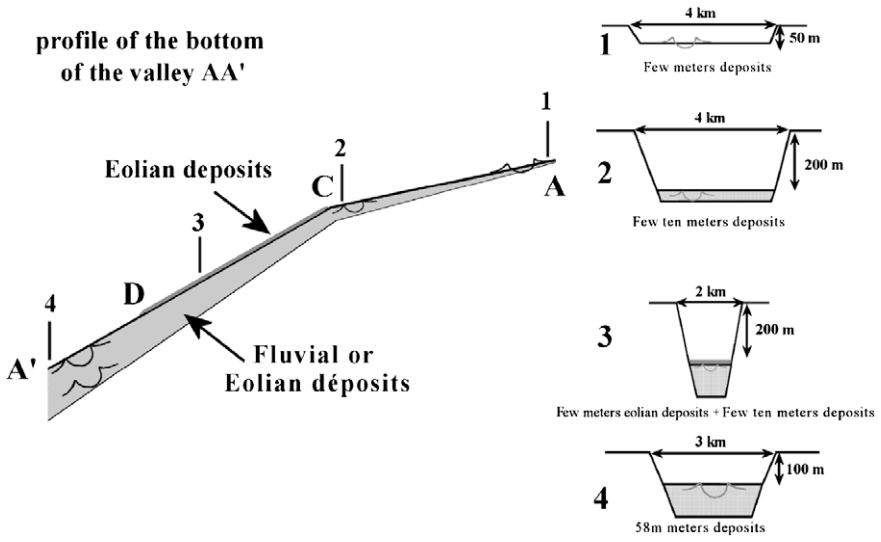

Fig. 15. Extrapolated profile of the bottom of the valley AA′ showing the variation of fluvial sediments thickness and the location of eolian deposits. For four different points, we show the cross section of the valley showing the filling thickness.

(2) Crater densities measured inside valleys using the high-resolution technique can be influenced by subsequent processes, such as eolian deposition, that are unrelated to the processes responsible for valley network formation. However, we were able to extract information related to the cessation of fluvial activity and use this technique to determine the thickness of subsequent deposition where it seemed to have been emplaced within the valley networks. This technique is useful for studying spatial variations of crater densities within the valley, but geomorphic analyses should be included to help interpret the crater density variations.
(3) In general the basin technique provides a more reliable maximum age estimate providing there is sufficient image resolution. It requires an extra step in determining the location of the drainage divides and it takes longer to apply because of the larger number of craters to count. However, it is useful when conducting regional studies, in characterizing the fluvial activity of a given network, and for observing spatial variations of resurfacing within the sub-basins. Generally, it has greater ability for obtaining the maximum age and can also help ascertain the validity of other techniques, which should always provide a younger or comparable age.

In summary, we can better understand the evolution of valley networks by applying all the techniques discussed here. Dating valley networks by a single technique alone will always provide some ambiguity because it will not take into account the variability of processes inside the basin as well as potential variations in subsequent activity that may have occurred both within the valley networks and the surround catchment.

8.2. Modification processes

Spatial variations of crater densities inside valleys and the sub-basins show that the thickness of the deposit and erosional effectiveness are heterogeneous. This heterogeneity can be explained by an effect of the distance to the source and maybe the local lithology. We showed that the thicknesses of the deposit increases downstream. The origin of downstream deposits may include both (1) a fluvial erosion of the upstream valleys and eroded upstream terrains and (2) an eolian or fluvial erosion of downstream plateaus surrounding valleys.

8.3. Parana network formation

Our study shows that Parana Valles ceased fluvial activity during the Early to Late Hesperian, which seems late compared to a majority of valley network ages determined in other studies. However, this age agrees with age estimates of several other networks, such as Naktong Vallis (Fassett and Head, 2008; Bouley et al., 2009) and Warrego Vallis (Ansan and Mangold, 2006). This suggests that several valley networks within the martian highlands were active up until the Hesperian. It should be noted that the Hesperian age of Parana Valles was provided by the high-resolution technique. However, the "high resolution dating technique" and the "basin technique" give the same results for crater between 500 m and 1 km of diameter. This range of diameter is the optimum sampling to determine the true age of Parana Valles formation. These craters are large enough not to be affected by eolian process and are numerous enough to provide reliable estimates of the absolute age. However, while these techniques can be applied to the Parana Valles drainage basin, it is important to point out that elsewhere on Mars this may not always be the case. The reliability of the techniques is sensitive to the intensity of subsequent modification processes and the thickness of any local aggradational material. In most instances, it is probably best to apply all three techniques when studying a particular valley network system to better understand the complete hydrologic history of the drainage basin and to fully assess subsequent modification processes within the area.

Acknowledgments

We gratefully acknowledge valuable discussions with Caleb Fassett, Monica Hoke, and Brian Hynek at the Second Workshop on Mars Valley Networks. Ana Baptista and Cathy Quantin provided useful comments throughout the preparation of this manuscript. This research was supported by NASA Grant NNX09AI40G (Mars Data Analysis Program) and the French Projet National de Planétologie (PNP) of the INSU (Institut des Sciences de l'Univers) France and CNES (Centre National d'Etudes Spatiales).

References

Ansan, V., Mangold, N., 2006. New observations of Warrego Valles, Mars: Evidence for precipitation and surface runoff. Planet. Space Sci. 54, 219–242.
Barnhart, C.J., Howard, A.D., Moore, J.M., 2009. Long-term precipitation and late-stage valley network formation: Landform simulations of Parana Basin, Mars. J. Geophys. Res. 114, E01003. doi:10.1029/2008JE003122.
Bouley, S., Ansan, V., Mangold, N., Masson, Ph., Neukum, G., 2009. Fluvial morphology of Naktong Vallis, Mars: A late activity with multiple processes. Planet. Space Sci. 57 (8–9), 982–999.
Carr, M.H., 1981. The Surface of Mars. Yale University Press, New Haven, Conn. pp. 65–70.
Carr, M.H., 1995. The martian drainage system and the origin of networks and fretted channels. J. Geophys. Res. (Planets) 100, 7479–7507. doi:10.1029/95JE00260.
Carr, M.H., 1996. Water on Mars. Oxford Univ. Press, New York. 229pp.
Carr, M.H., Clow, G.D., 1981. Martian channels and valleys: Their characteristics, distribution, and age. Icarus 48, 91–117.
Christensen, P.R., and 21 colleagues, 2003. Morphology and composition of the surface of Mars: Mars Odyssey THEMIS results. Science 300 (5628), 2056–2061.
Costa-Cabral, M.C., Burges, S.J., 1994. DEMON (Digital Elevation Model Networks): A model of flow over hillslopes for computation of contributing and dispersal areas. Water Resour. Res. 30 (6), 1681–1692.
Craddock, R.A., Howard, A.D., 2002. The case for rainfall on a warm, wet early Mars. J. Geophys. Res. 107 (5111), 1–36.
Duxbury, T.C., Kirk, R.K., Archinal, B.A., Neumann, G.A., 2002. Mars geodesy/cartography working group recommendation on Mars cartographic constants and coordinate systems. In: Symposium on Geospatial Theory. Processing and Application. Ottawa.
Fassett, C.I., Head III, J.W., 2008. The timing of martian valley network activity: Constraints from buffered crater counting. Icarus 195, 61–89.
Garbrecht, J., Martz, L.W., 1997. The assignment of drainage direction over flat surfaces in raster digital elevation models. J. Hydrol. 193, 204–213.
Garvin, J., 2002. Global geometric properties of martian impact craters. Proc. Lunar Sci. Conf. 33. Abstract 1255.
Goldspiel, J.M., Squyres, S.W., 1991. Ancient aqueous sedimentation on Mars. Icarus 89, 392–410.
Grant, J.A., 1987. The geomorphic evolution of eastern Margaritifer Sinus, Mars. In: Advances in Planetary Geology. NASA Tech. Memo., TM-89871, pp. 1–268.
Grant, J.A., Parker, T.J., 2002. Drainage evolution in the Margaritifer Sinus region, Mars. J. Geophys. Res. 107 (E9), 5066. doi:10.1029/2001JE001678.
Greeley, R., Guest, J.J., 1987. Geologic map of the eastern equatorial region of Mars. Maps 1:15,000,000. USGS Maps I-1802-B.
Gulick, V.C., 2001. Origin of the valley networks on Mars: A hydrological perspective. Geomorphology 37, 241–268.
Hartmann, W.K., 2005. Martian cratering 8: Isochron refinement and the chronology of Mars. Icarus 174, 294–320.
Hartmann, W.K., Neukum, G., 2001. Cratering chronology and evolution of Mars. Space Sci. Rev. 96 (1–4), 165–194.
Hoke, M.R.T., Hynek, B.M., 2008. Analyzing and dating valley networks in Arabia Terra and Terra Meridiani, Mars. Lunar Planet. Sci. Abstract 2183.
Horton, R.E., 1945. Erosional development of streams and their drainage basin. Hydrophysical approach to quantitative morphometry. Geol. Soc. Am. Bull. 56, 275–370.
Howard, A.D., Moore, J.M., Irwin III, R.P., 2005. An intense terminal epoch of widespread fluvial activity on early Mars: 1. Valley network incision and associated deposits. J. Geophys. Res. 110, E12S14. doi:10.1029/2005JE002459.
Irwin III, R.P., Howard, A.D., Craddock, R.A., Moore, J.M., 2005. An intense terminal epoch of widespread fluvial activity on early Mars: 2. Increased runoff and paleolake development. J. Geophys. Res. 110 (E12).
Malin, M.C., and 13 colleagues, 2007. Context Camera investigation on board the Mars Reconnaissance Orbiter. J. Geophys. Res. 112, E05S04. doi:10.1029/2006JE002808.
Mangold, N., Quantin, C., Ansan, V., Delacourt, C., Allemand, P., 2004. Evidence for precipitation on Mars from dendritic valleys in the Valles Marineris area. Science 305, 78–81.

Mangold, N., Ansan, V., Mason, Ph., Vincendon, C., 2009. Estimate of eolian thickness in Arabia Terra, Mars: Implications of a thick mantle (>20 m) for hydrogen detection. Géomorphologie 1, 23–32.
Mars Channel Working Group, 1983. Channels and valleys on Mars. Geol. Soc. Am. Bull. 94, 1035–1054.
Martz, L.W., Gabrecht, J., 1992. Numerical definition of drainage networks and subcatchment area from digital elevation models. Comput. Geosci. 18, 747–761.
McEwen, A.S., 2003. Secondary cratering on Mars: Implications for age dating and surface properties. In: Mars Polar Ice Conference 3rd, Lake Louise, Canada, October, 2003. Abstract 3268.
McEwen, A.S., Turtle, E., Burr, D., Milao, M., Lanagan, P., Christensen, P., Boyce, J., 2003. Discovery of a large rayed crater on Mars: Implications for recent volcanic and fluvial activity and the origin of martian meteorites. Lunar Planet. Sci. XXXIV. Abstract 2040.
Milton, D.J., 1973. Water and processes of degradation in the martian landscape. J. Geophys. Res. 78, 4037–4047.
Nakimi, K., Solomon, S.C., 1994. Impact crater densities on volcanoes and coronae on Venus: Implications for volcanic resurfacing. Science 265, 929–933.
Palacios-Velez, O., Cuevas-Renaud, B., 1986. Automated river-course, ridge and basin delineation from digital elevation data. J. Hydrol. 86, 299–314.
Pieri, D.C., 1976. Distribution of small channels on the martian surface. Icarus 27, 25–50.
Quantin, C., Craddock, R.A., 2008. Timing of martian valley network using fine scale age determination. In: Second Workshop on Valley Networks, Moab, Utah, pp. 59–61.
Quantin, C., Allemand, P., Mangold, N., Dromart, G., Delacourt, C., 2005. Fluvial and lacustrine activity on layered deposits in Melas Chasma, Valles Marineris, Mars. J. Geophys. Res. 110 (E12).
Schultz, P.H., Ingerson, F.E., 1973. Martian lineaments from Mariner 6 and 7 images. J. Geophys. Res. 78, 8385–8415.
Scott, D.H., Dohm, J.M., 1992. Mars highland channels: An age reassessment. Lunar Planet. Sci. XXIII, 1251–1252.
Scott, D.H., Tanaka, K.L., 1986. Geological map of the western equatorial region of Mars (1:15,000,000). US Geol. Surv. Scientific Investigations I-1802-A.
Scott, D.H., Dohm, J.M., Rice, J.W., 1995. Map of Mars showing channels and possible paleolake basins. USGS Misc. Inv. Ser. Map I-2461.
Sharp, R.P., Malin, M.C., 1975. Channels on Mars. Geol. Soc. Am. Bull. 86, 593–609.
Shreve, R.L., 1967. Infinite topologically random channel networks. J. Geol. 75, 178–186.
Smith, D.E., Sjogren, W.L., Tyler, G.L., Balmino, G., Lemoine, F.G., Konopliv, A.S., 1999. The gravity field of Mars: Results from Mars Global Surveyor. Science 286, 94–97.
Strahler, A.N., 1952. Dynamic basis of geomorphology. Geol. Soc. Am. Bull. 63, 923–938.
Tanaka, K.L., 1982. A new time-saving crater-count technique with application to narrow features. NASA Tech. Memo., TM-85127, pp. 123–125.
Tanaka, K.L., 1986. The stratigraphy of Mars. Proc. Lunar Sci. Conf. 17, Part 1, J. Geophys. Res. 91 (Suppl.), E139–E158.
Tarboton, D.G., 1997. A new technique for the determination of flow directions and contributing areas in grid digital elevation models. Water Resour. Res. 33 (2), 309–319.
Wichman, R.W., Schultz, P.H., 1989. Sequence and mechanisms of deformation around the Hellas and Isidis impact basins on Mars. J. Geophys. Res. 94, 17333–17357.
Zhang, W., Montgomery, D.R., 1994. Digital elevation model grid size, landscape representation, and hydrologic simulations. Water Resour. Res 30 (4), 1019–1028.